Downsizing FeNb11O29 anode material through ultrafast solid-state microwave-assisted synthesis for enhanced electrochemical performance

Dat Le Thanh, Amandine Guiet, Emmanuelle Suard, Romain Berthelot

Downsizing $FeNb_{11}O_{29}$ anode material through ultrafast solid-state microwave-assisted synthesis for enhanced electrochemical performance

Authors: Dat Le Thanh[1,2,3], Amandine Guiet[4], Emmanuelle Suard[1], Romain Berthelot[2,5]*

1: Institut Laue-Langevin (ILL), BP 156, 71 Avenue des Martyrs, Grenoble 38042, France

2: ICGM, Univ Montpellier, CNRS, ENSCM, Montpellier 34095, France

3: Alistore-European Research Institute, CNRS FR 3104, Hub de l'Energie, Amiens 80039, France

4: Institut des Molécules et Matériaux du Mans (IMMM), UMR 6283 CNRS, Le Mans Université, Avenue Olivier Messiaen, 72085 Le Mans, France

5: Réseau sur le Stockage Électrochimique de l'Énergie (RS2E), CNRS, Amiens 80000, France

Corresponding author:

romain.berthelot@umontpellier.fr

Keywords: Wadsley-Roth phase, microwave synthesis; anode material; particle downsizing

Abstract

Wadsley-Roth oxide $FeNb_{11}O_{29}$ powder samples are successfully prepared using a simple, cost-effective, and ultrafast microwave-assisted solid-state synthesis for the first time. While conventional solid-state route in furnace requires hours of high-temperature treatment, both monoclinic and orthorhombic polymorphs of $FeNb_{11}O_{29}$ were obtained in minutes under microwave heating. Combining such short heat treatment with submicrometric oxide precursors enables to limit particle growth during the synthesis. The electrochemical benchmark clearly shows that $FeNb_{11}O_{29}$ powder samples obtained rapidly from submicrometric oxide precursors exhibit enhanced cycling performance. For example, the

monoclinic polymorph prepared in only 5 minutes offers a high capacity of 179 mAh g^{-1} (90 % retention) after 500 cycles at 2 A g^{-1}, approximately 20 % more than with conventional synthesis protocol. Electrochemical analysis demonstrates that the extra capacity is gained at low voltage and is probably induced by an easier ionic diffusion occurring in smaller particles. This work confirms the interest of solid-state microwave heating to design of electrode materials with limited particles growth and better cycling performance.

Graphical Abstract

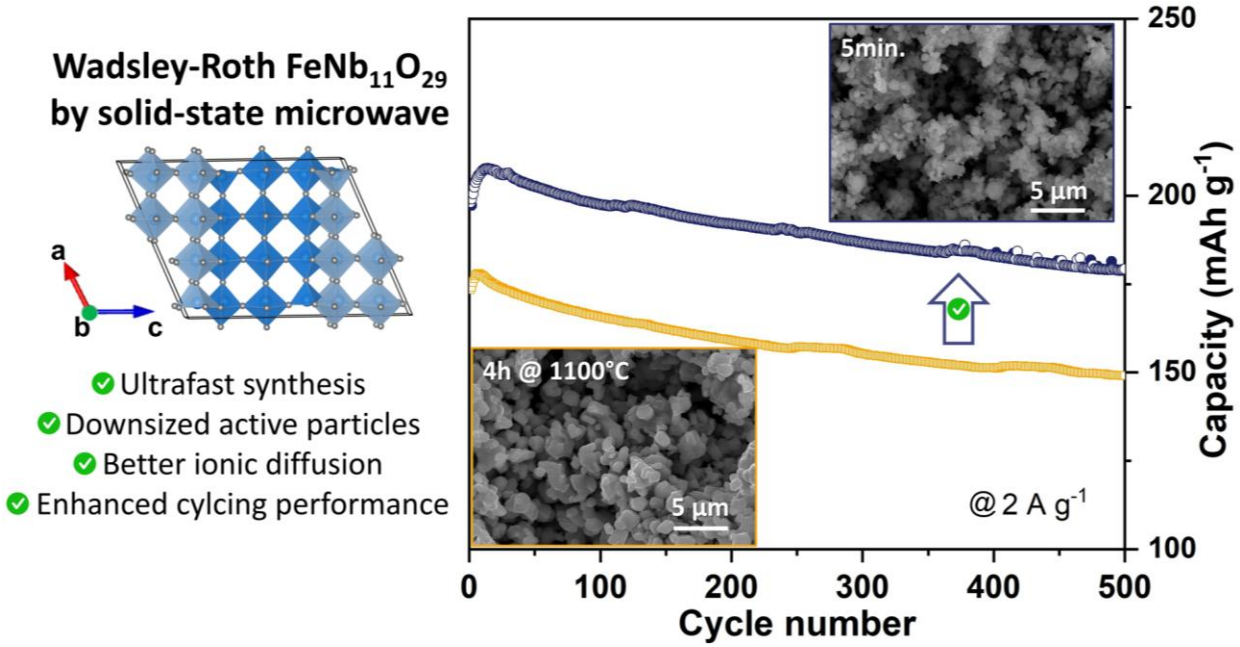

1. Introduction

Next generation of electrode materials for Li-ion batteries requires not only high capacity and durable cyclability but also high performance (capacity, cyclability) at elevated currents, especially for power-intensive applications. The intercalation-type graphite and $Li_4Ti_5O_{12}$ are commonly used in commercial lithium-ion batteries yet certain limitations remain. While graphite offers high electronic conductivity and theoretical capacity of 372 mAh g^{-1} via the formation of LiC_6, there are concerns about its limited rate capability due to the formation of a passivating solid-electrolyte interphase (SEI) with slow Li^+ diffusion kinetics. Besides, graphite also poses the risks of lithium electroplating at high currents because of its low lithiation potential (around 0.1 V *vs.* Li^+/Li) [1]. Spinel $Li_4Ti_5O_{12}$, with moderate lithiation potential (plateau at 1.5 V), exhibits better rate performance with no SEI but still unsatisfactory capacity of 175 mAh g^{-1} [2]. In this context, niobium-based oxides with Wadsley-Roth crystallographic shear structure are a well-known family of compounds [3–6] and have sparked considerable interest as alternative negative electrode materials with high capacities especially at elevated current rate [7–12]. These compounds bring about the advantage of minimizing the risk of side reactions with conventional organic carbonate-based electrolytes and mitigating the formation of lithium dendrites thanks to their operating voltage above 1 V. Notably, $Nb_{12}O_{29}$ possesses robust structure of $n \times m$ octahedron-blocks and large insertion channels along *b* direction for facile Li^+ diffusion. Partial substitution of niobium gives the analogous compounds such as $FeNb_{11}O_{29}$, $CrNb_{11}O_{29}$ with improved electronic conduction [13–17]. However, their electronic and ionic conductivities are still insufficient for the full exploitation of their capacity, and extensive improvement space for electrochemical kinetics is therefore still available [7].

In this work, we focus our effort on the Wadsley-Roth oxide $FeNb_{11}O_{29}$, which exists in two polymorphs. According to the literature, the monoclinic form of $FeNb_{11}O_{29}$ is formed at temperature of 900-1100 °C, while the orthorhombic polymorph is obtained at 1250 °C through an irreversible phase transition [18–21]. Both phases are constructed from blocks of 4×3 $Nb(Fe)O_6$ octahedra which are corner-connected within one individual block. The interblock connection is made by edge-sharing of octahedra, creating crystallographic shear planes to accommodate the oxygen deficiencies. The subtle structural change between the two polymorphs lies on the linkage of blocks at the same level, sharing *cis* or *trans* corners in orthorhombic and monoclinic forms, respectively [18–21]. Neutron powder diffraction, Mössbauer spectroscopy and X-ray absorption spectroscopy have confirmed the fully disordered distribution of Fe and Nb within six crystallographic sites [17,22].

Both polymorphs of $FeNb_{11}O_{29}$ can theoretically exchange up to 23 electrons per formula unit, thanks to the three redox couples of Fe^{3+}/Fe^{2+}, Nb^{5+}/Nb^{4+}, and Nb^{4+}/Nb^{3+}, which correspond to a high theoretical capacity of 400 mAh g^{-1} [18–21]. This value is higher than that of $Li_4Ti_5O_{12}$ and graphite, making $FeNb_{11}O_{29}$ a promising anode material. However, their practical capacity significantly differs in the literature. For example, the orthorhombic polymorph obtained by conventional furnace treatment was reported to deliver up to 400 mAh g^{-1} at 0.1 A g^{-1} [23], whereas all other research showed lower capacity in the range of 250-300 mAh g^{-1}, depending on the synthesis protocol [23]. The electrochemical difference between the two polymorph was investigated only by Spada *et al.*, where monoclinic one mainly has the charge storage on the surface with higher pseudocapacitive contribution determined by cyclic voltammetry, leading to its lower specific capacity than orthorhombic one [23]. Different research directions have been followed to enhance the electrochemical performance of $FeNb_{11}O_{29}$, including partial substitution of iron with other transition metals such as Ti, V or Mn [19,24,25], creation of oxygen defects by annealing under vacuum or inert atmosphere [26], nitridation surface formation by treatment in Ar/NH_3 atmosphere [23], or nanostructuration by electrospinning [27].

As stated before, $FeNb_{11}O_{29}$ is usually obtained at high temperature, which could induce large particles and consequently prevent an efficient ionic diffusion and alter the electrochemical performance. Herein, we investigate microwave-assisted solid-state protocol with the objective of downsizing the particle size of $FeNb_{11}O_{29}$. This synthesis method is based on the interaction between samples and the electromagnetic field to directly convert microwave into thermal energy, resulting in uniform heating in the sample volume and rapidly rising temperature for the reaction to occur. The ultrafast heating is known to offer the possibility of decreasing the particle size and has been adapted for a wide range of inorganic compounds [28], especially for battery electrode and electrolyte materials such as Chevrel phase $Cu_2Mo_6S_8$, disordered rocksalt $Li_{1.3}Mn_{0.4}Nb_{0.3}O_{1.9}F_{0.1}$ and thiophosphate solid electrolyte Na_3PS_4, with comparable performance as those obtained by conventional method [29–32]. Concerning Wadsley-Roth phases, only microwave-assisted solvothermal method was used to prepare $TiNb_2O_7$ [26], whereas microwave-assisted solid-state synthesis has not been applied to the best of our knowledge. For the first time, we show here that it is possible to prepare $FeNb_{11}O_{29}$ in a few minutes of heating, and we take advantage of this fast process to obtain the product of smaller particles, which can facilitate lithium diffusion and enhance electrochemical performance.

2. Experimental

Stoichiometric amounts of oxide precursors Fe_2O_3 (≥ 99 %, < 5 µm, Honeywell) and Nb_2O_5 (obtained by heating Nb powder (99.8 %, ~ 325 mesh, Alfa Aesar) at 900 °C for 24 h), weighed around 2 g, were mixed in SPEX 8000M high-energy ball mill for 20 minutes. The mixture was recovered and then pelletized under 2 t in a hydraulic press. In conventional solid-state synthesis, the pellets were heated in air in Nabertherm muffle furnace for 4 h at 1100 or 1300 °C (with a heating rate of 2 °C min^{-1}) to obtain either the monoclinic or orthorhombic polymorphs, respectively. A second series of synthesis have been carried out similarly with submicrometric oxide precursors Fe_2O_3 (99.9 %, 80 nm, Nanoshel) and Nb_2O_5 (99.9 %, 80-100 nm, Nanoshel). In a typical microwave-assisted solid-state synthesis, the pellet of mixed oxide precursors, weighed around 0.5 g, was put inside a graphitized quartz tube placed in a porcelain crucible filled with thermally conductive carbon powder (C-NERGY Super C45) and covered by mineral wool (5-30 µm, Sodipro). The heat treatment was conducted in a classic kitchen microwave oven at 1200 W during one or subsequent steps of 5 minutes, with intermediate resting time to avoid overheating and possible irreversible damage of the quartz tube. At the end, the tube was kept inside the oven to cool down gradually. The as-obtained pellets were manually ground in an agate mortar into fine powder for further characterization and electrochemical evaluation. Overall, eight powder samples were obtained and were labeled according to the series of oxide precursors (micrometric -*µ*- or submicrometric -*sµ*-), the thermal treatment (furnace -*f*- or microwave -*w*-), and finally the polymorph (monoclinic -M- or orthorhombic -O-).

X-ray powder diffraction (XRPD) patterns were collected by using a 2θ/θ diffractometer (Empyrean, PANAlytical) with Co Kα radiation source. Scanning Electron Microscopy (SEM) images were obtained by using a JEOL microscope (JSM 6510 LV) at 20 kV. All samples were coated with gold before analysis. The mean particle size was deduced by statistical evaluation of about 100 particles using ImageJ software.

Regarding electrode preparation, the active materials ($FeNb_{11}O_{29}$ powders) were manually ground with carbon additive (Super P) and polymeric binder (polyvinylidene fluoride, Solef 5130) in the weight proportions of 70:20:10. Then, N-methyl-pyrrolidone (99.5 %, Sigma-Aldrich) solvent was added and the resulting mixture was subsequently placed inside a planetary centrifugal mixer (SK-300SII, Kakuhunter). The obtained slurry was coated onto Cu foil (Goodfellow, thickness of 0.02 mm) and dried under vacuum at 80 °C for 12 h. Finally, 12.7 mm disc electrodes were cut from the foil. The electrode thickness was measured around 50 µm (excluding the Cu foil), corresponding to a mass loading of active material between 1.8 and 2.2 mg cm^{-2}. Coin cells were assembled inside Ar-filled glovebox with metallic lithium as

anode, glass fiber separator (Whatman grade D) and 1M $LiPF_6$ in EC:DMC (3:7 vol.%) (Solvionic) as electrolyte.

Electrochemical measurements have been performed at room temperature using potentiostats (MPG-2 and VMP, Bio-Logic). With the capacity C set at 208.6 mAh g^{-1} (corresponding to the insertion if 12 lithium ions per formula unit), galvanostatic cycling with potential limitation (GCPL) was carried out at 10 C between 1.0 V and 3.0 V *vs.* Li^+/Li, while rate capability tests were conducted from C/2 to 100 C and back to C/2. Galvanostatic Intermittent Titration Technique (GITT) was done for the monoclinic polymorphs of $FeNb_{11}O_{29}$ obtained from submicrometric precursors either with conventional or microwave heat treatment, with C/20 current pulses of 10 minutes followed by relaxation of 20 minutes. These two samples were also investigated by Electrochemical Impedance Spectroscopy (EIS) at room temperature, in the frequency range between 10^4 Hz and 10^{-2} Hz, with the amplitude of perturbative sinusoidal wave as 10 mV, during open circuit voltage, at the end of discharge and end of charge. The first cycle at C/2 was scrutinized by *operando* X-ray diffraction for electrodes containing powder samples obtained by microwave heating, using the above-mentioned diffractometer and a home-made electrochemical cell.

3. Results and discussion

At first, conventional solid-state synthesis in muffle furnace was used to prepare $FeNb_{11}O_{29}$ reference samples. Whatever the particle size of the oxide precursors, Fe_2O_3 and Nb_2O_5, (micrometric or submicrometric), the heat treatments performed at 1100 °C lead to the monoclinic form of $FeNb_{11}O_{29}$, with XRPD pattern indexed in the space group *A*2/*m*, while going up to 1300 °C induces the formation of the orthorhombic polymorph (space group *Amma*), as shown in Figure S1. In both cases, cell parameters obtained from profile matching refinement of XRPD data (Table S1) are in good agreement with the literature [19,20,23].

In parallel, microwave-assisted thermal treatment has been applied on both micrometric and submicrometric oxide precursors. The mixture was heated during four steps of five minutes each, at 1200 W, and XRPD was performed after each step to monitor the chemical reaction (Figure S2). With the micrometric precursors, after only 5 minutes the main peak of monoclinic $FeNb_{11}O_{29}$ at 28 ° is observed. However, another peak at 36 ° is present and assigned to $FeNbO_4$, which has been evidenced as an intermediate phase during *in situ* high temperature X-ray diffraction (Figure S3). After a third heating step, $FeNbO_4$ is no longer present and pure monoclinic form of $FeNb_{11}O_{29}$ is observed. An additional step

is necessary to obtain the orthorhombic polymorph. The use of submicrometric oxide precursors Fe_2O_3 and Nb_2O_5 enables to shorten the synthesis duration. Indeed, pure and highly crystalline monoclinic form of $FeNb_{11}O_{29}$ is obtained after one heating step of 5 minutes, and the orthorhombic polymorph only need an additional step to be observed (Figure 1).

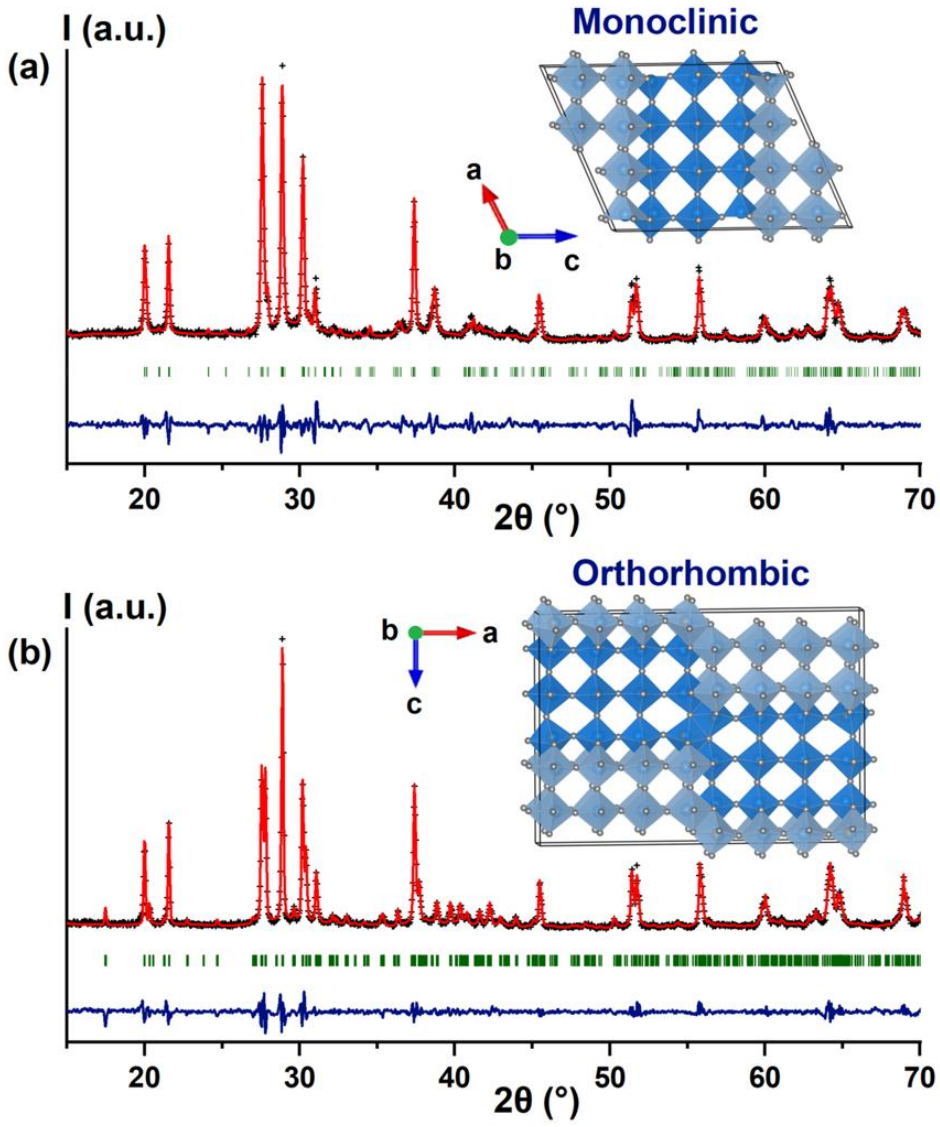

Figure 1. *XRPD patterns and crystallographic structures of (a) monoclinic and (b) orthorhombic* $FeNb_{11}O_{29}$ *samples, obtained by microwave heat treatment of submicrometric precursors in 5 or 10 minutes, respectively (observed, Le Bail-fitted and difference profile are represented respectively on black crosses, red and blue lines, and Bragg position on green vertical bars). The dark and light shades of blue are used to distinguish different layers stacked along the b direction.*

SEM is used to study the influence of three synthesis parameters on the particle size of $FeNb_{11}O_{29}$ powder, and images of all samples of $FeNb_{11}O_{29}$ are compared in Figures 2, S4 and S5 for different magnifications. First, it is important to mention that Energy Dispersive X-ray spectroscopy (EDX) coupled SEM confirms the Nb/Fe ratio and the homogeneous elemental distribution in the samples, shown in Figure S6. Comparing between the two polymorphs of $FeNb_{11}O_{29}$, it is reasonable to claim that the four orthorhombic samples – synthesized either at higher temperature or during a longer treatment time under microwave – have significant particle growth with respect to the monoclinic ones. Focusing on the heating process, the four samples obtained from microwave method show the aggregation of small primary particles (diameter ≈ 0.5 µm) into larger secondary assembly, while powder samples heated hours in furnace are characterized by larger particles (diameter ≈ 2 µm) and smooth surface. Finally, for a similar heating process, using submicrometric oxide precursors allows to limit the grain growth. Logically, the combination of these precursors with the rapid microwave-assisted synthesis remarkably limits particle growth and yields the product with a limited particle size. This is particularly evidenced with the monoclinic form of $FeNb_{11}O_{29}$ obtained in only 5 minutes and exhibiting particle size of 0.3-0.5 µm, slightly larger than its oxide precursors.

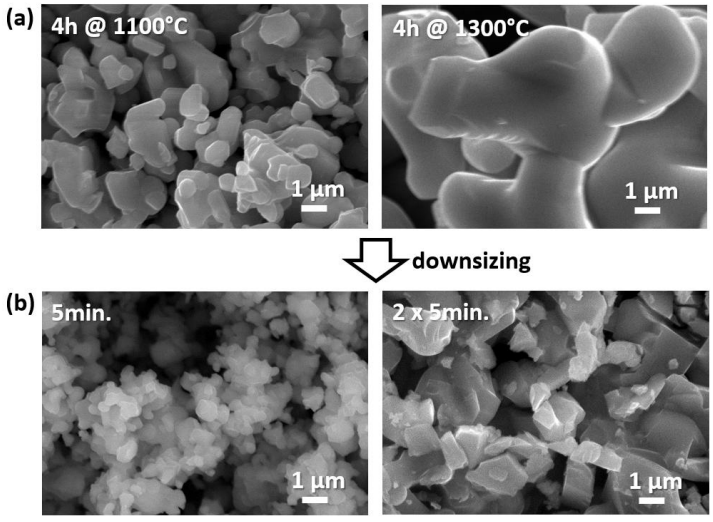

Figure 2. *SEM images showing how $FeNb_{11}O_{29}$ particles could be downsized from a conventional heat treatment with micrometric Fe_2O_3 and Nb_2O_5 precursors (a) to an ultrafast microwave heating with submicrometric precursors (b). In both cases, left and right images correspond to monoclinic and orthorhombic polymorphs of $FeNb_{11}O_{29}$, respectively. Additional SEM images for other $FeNb_{11}O_{29}$ batches and with different magnifications are provided in the SI section.*

The electrochemical behavior of the eight $FeNb_{11}O_{29}$ samples has been evaluated in the same conditions, from the electrode formulation to the cycling conditions. The first galvanostatic cycles at C/2 are compared in Figure 3. For the monoclinic polymorphs, the discharge/charge curves are very similar and start by short pseudoplateau at 2.4 V, followed by a more apparent yet sloping plateau around 1.6 V. A total of 14 Li^+ ions per formula unit could be inserted, corresponding to a capacity of 243 mAh g^{-1}, and with an excellent reversibility observed during the subsequent charge. The corresponding differential capacity plots distinguish three redox reactions. Following previous works [19,20,23,27], the first faint broad cathodic/anodic peak around 2.4 V is assigned to Fe^{3+}/Fe^{2+} redox couple. The important peaks around 1.6-1.7 V correspond to Nb^{5+}/Nb^{4+} redox couple, whereas the broad features below 1.5 V are attributed to further redox activity of Nb^{4+}/Nb^{3+}. Interestingly, a significant extra capacity is observed with the sample prepared by microwave heating from the submicrometric oxide precursors (*sμ-w*-M) and this gain is occurring below 1.25 V. These observations slightly differ for the orthorhombic samples of $FeNb_{11}O_{29}$. A stronger polarization is observed below 1.5 V and induces a lower discharge capacity as only 12 Li^+ could be inserted. This decrease of capacity is however not noticed for the sample prepared by microwave heating from the submicrometric oxide precursors (*sμ-w*-O), and here as well this extra capacity seems to be explained by a stronger activity at low voltage.

As stated in the introduction, Wadsley-Roth phases recently focused the spotlight thanks to their good electrochemical activity especially at high current rates. Consequently, rate-capability tests have been applied to the $FeNb_{11}O_{29}$ electrodes (Figure 3). Clearly, samples prepared from micrometric oxide precursors offer weaker capability retention whatever the polymorph considered. The extra capacity gained at C/2 for the samples prepared by microwave heating from submicrometric oxide precursors (*sμ-w*-M and *sμ-w*-O) is still observed and interestingly even more pronounced at higher current rates. Finally, long-term cycling tests have been carried out at 10 C (Figure 3). The better electrochemical behavior of the two microwave-heated samples with submicrometric oxide precursors is unambiguously highlighted. The monoclinic form of $FeNb_{11}O_{29}$ exhibits the best cycling performance, delivering 198 mAh g^{-1} initially and retaining a capacity of 90.4 % after 500 cycles (179 mAh g^{-1}) and 77 % after 1300 cycles (153 mAh g^{-1}). This highest initial capacity at 10 C in the present work is even superior to the values previously reported for the best $FeNb_{11}O_{29}$-based materials enhanced by different strategies, *e.g.* 170 mAh g^{-1} for the monoclinic doped sample $Fe_{0.67}Ti_{0.67}Nb_{10.67}O_{29}$ or 150 mAh g^{-1} delivered by monoclinic $FeNb_{11}O_{29}$ nanotubes. However, more effort is still needed to improve the long-term cycling and capacity retention of our materials. Comparing between two polymorphs in this work, monoclinic samples with smaller particle size show higher long-term capacity and better rate capability with respect to

orthorhombic ones. This result, however, is contrary to the study by Spada *et al.* [23], as mentioned in the introduction part, with 200 mAh g^{-1} and 130 mAh g^{-1} delivered at 10 C by the orthorhombic and monoclinic sample, respectively.

The overall superior performance of microwave-heated samples can be explained by a smaller particle size, allowing effective electrolyte impregnation, faster Li^+ diffusion and better material utilization during electrochemical cycling. To grasp further into the details of the electrochemical lithiation of $FeNb_{11}O_{29}$ and possibly confirm this initial assumption, GITT technique was implemented to study dynamic aspect of the material, *i.e.* diffusion behavior of lithium-ions, as well as EIS analysis and finally *operando* XRPD has been carried out to scrutinize the evolution of the cell parameters. This part of the investigation only focuses on the monoclinic polymorphs as they offer the best electrochemical performance.

At a first glance, a unique GITT profile is observed whatever the heating protocol (Figure 4). Consequently, the calculated diffusion coefficients of Li^+ ions are also close, remaining steadily high during the early stage of the discharge, followed by a sharp decrease from 1.8 to 1.5 V and then an increase till 1.2 V. However, the enhancement of the diffusion coefficient during the end of discharge (below 1.5 V) is unambiguously more pronounced for the electrode with active material prepared by microwave-assisted heating (*sμ-w*-M) and the situation remains in the subsequent charge until the voltage reaches 1.6 V. After that both electrodes exhibit a similar evolution. The higher lithium-ion diffusivity of the microwave-heated sample at low voltage echoes with its more intense differential capacity (dQ/dV) peak observed in Figure 3 in the same voltage range. Nyquist plots obtained from EIS experiments reveal lower values of electron transfer resistance for microwave-heated material compared with furnace-heated sample, which is in line with its smaller particles. This lower resistance is consistently observed at open circuit and all along the electrochemical cycle (Figure S7 and Table S2).

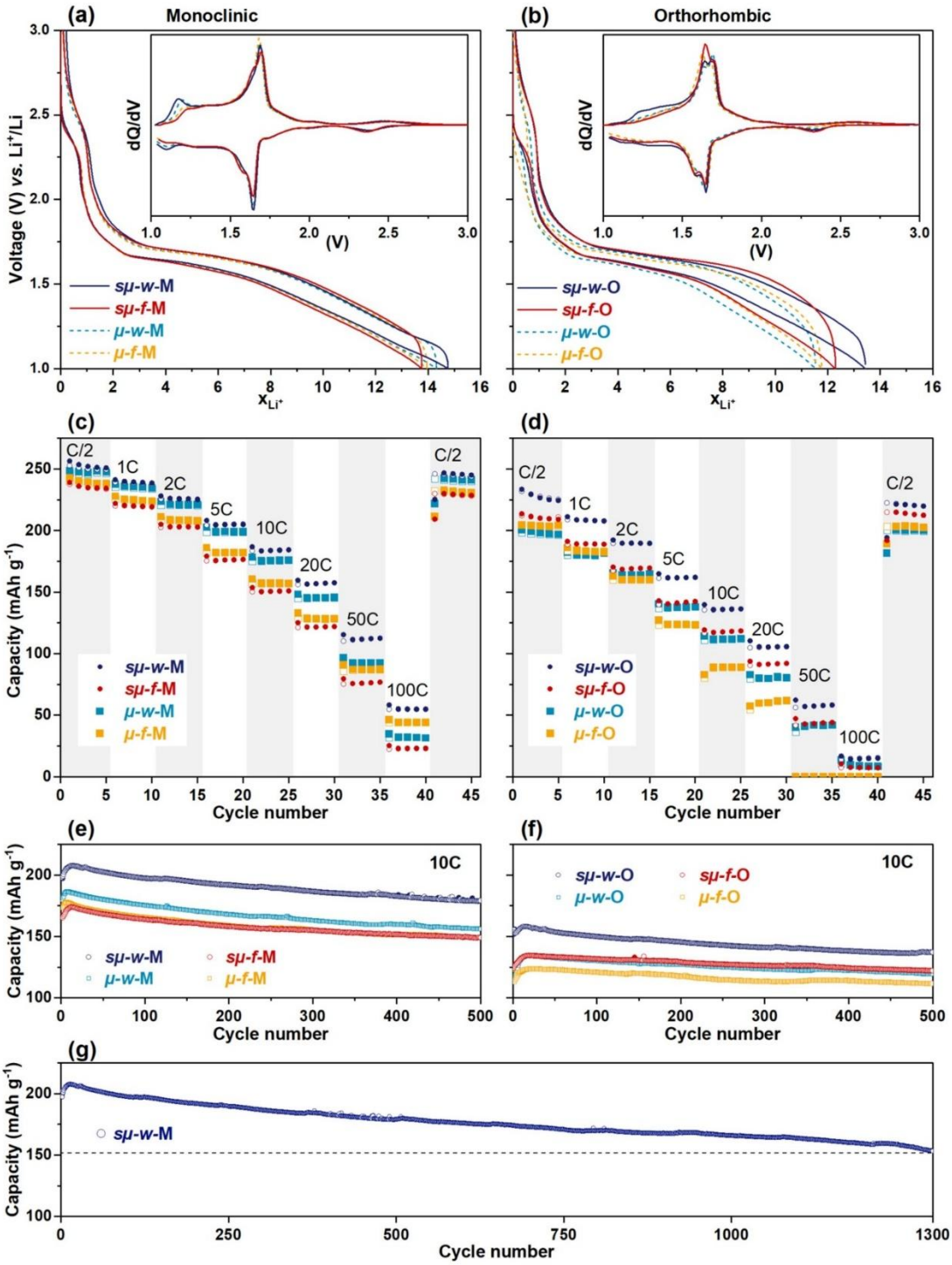

Figure 3. *Galvanostatic discharge-charge curves and differential capacity curves of eight* $FeNb_{11}O_{29}$ *samples in their first cycle at C/2 = 0.1 A* g^{-1} *(a-b), their rate capability tests from C/2 to 100 C (c-d), the comparison of their 500 galvanostatic cycles at 10 C (e-f), and long-term cycling of sμ-w-M sample at 10 C in 1300 cycles.*

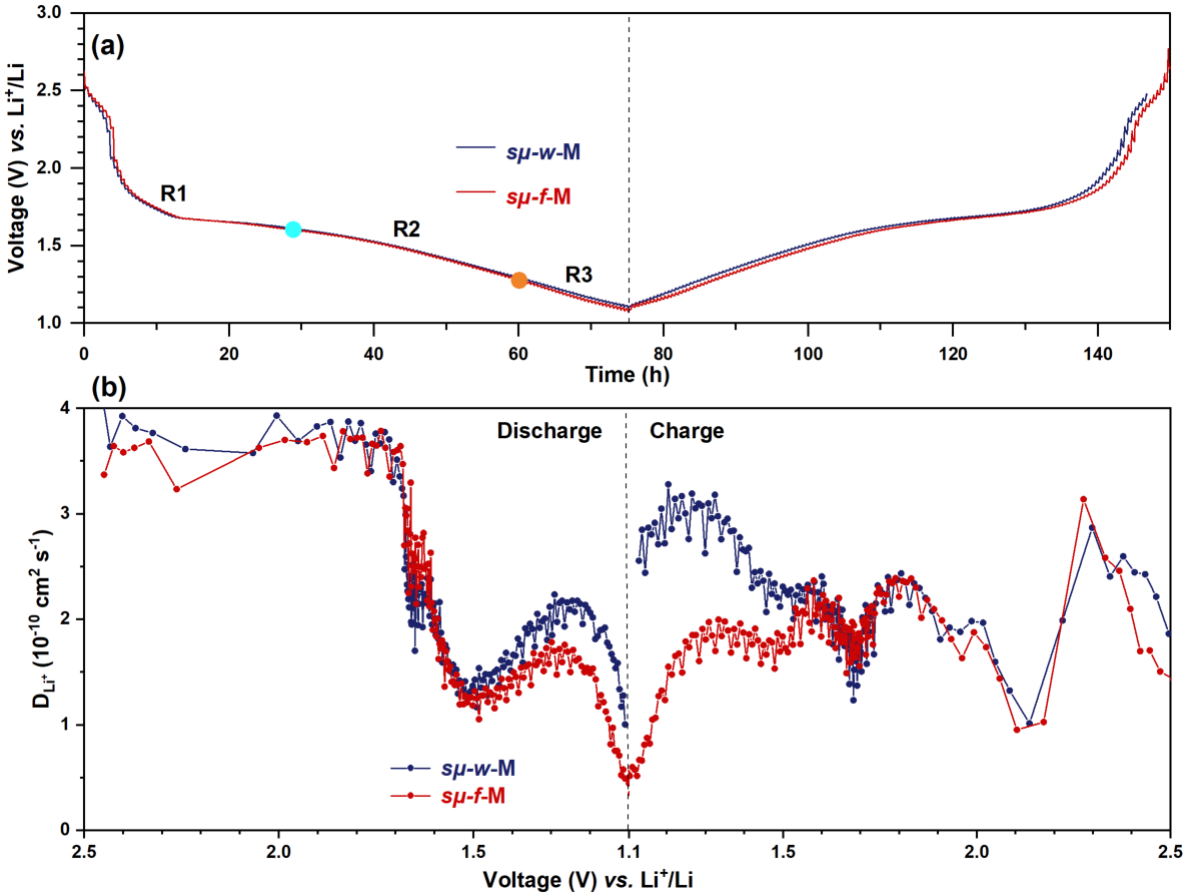

Figure 4. *GITT profiles of two samples prepared from submicrometric precursors: sμ-w-M and sμ-f-M, with three ranges of lithiation degree corresponding to the three-stage evolution of* (*a,c*) plane *(a), and the evolution of GITT-extracted* Li^+ *diffusion coefficient vs. voltage during discharge and charge (b).*

The evolution of the diffusion coefficient was compared with those of the cell parameters during the electrochemical process. Firstly, from the 2-dimensional contour plot of the XRD patterns, all the diffraction peaks evolve continuously and return to their initial positions without any newly appeared features during the whole discharge-charge process (Figure 5). The overall electrochemical process follows reversible lattice changes without any phase transformation or biphasic reaction as previously reported [23,27]. Secondly, the evolution of the cell parameter is scrutinized. Along the lithium insertion, the *b* parameter increases steadily and significantly, indicating that lithium ions diffuse along the channels perpendicularly to the block planes. Meanwhile, *a* and *c* parameters evolve in a more complex way, with an initial expansion of the (*a,c*) plane until around 1.4 V *vs.* Li^+/Li (region R1), which can be explained by Li^+-ion insertion in the structure. Afterwards, the (*a,c*) plane contracts until 1.2 V (region

R2) due to the enhanced electrostatic attraction between intercalated Li^+ and O^{2-} ions [23]. At the third stage of discharge, both parameters increase again (region R3), probably because of the reduction of niobium, from Nb^{4+} (68 pm) to Nb^{3+} (72 pm) [23]. This three-stage feature somehow mimics the evolution of lithium-ion diffusivity in similar ranges of lithiation degree as shown in Figure 4. This indicates the close relationship between the size of the diffusion channels and the diffusive behavior, where the expanded (*a*,*c*) plane results in faster diffusion of lithium-ions and *vice versa*.

Over the charge process, these lattice parameters undergo reverse evolutions and return to their original values, which further confirms the reversibility of the reactions. Overall, unit-cell volume expansion after full lithiation is 5.4 %. This low value appears in line with the literature [27] and also contributes to the long-term cycling stability.

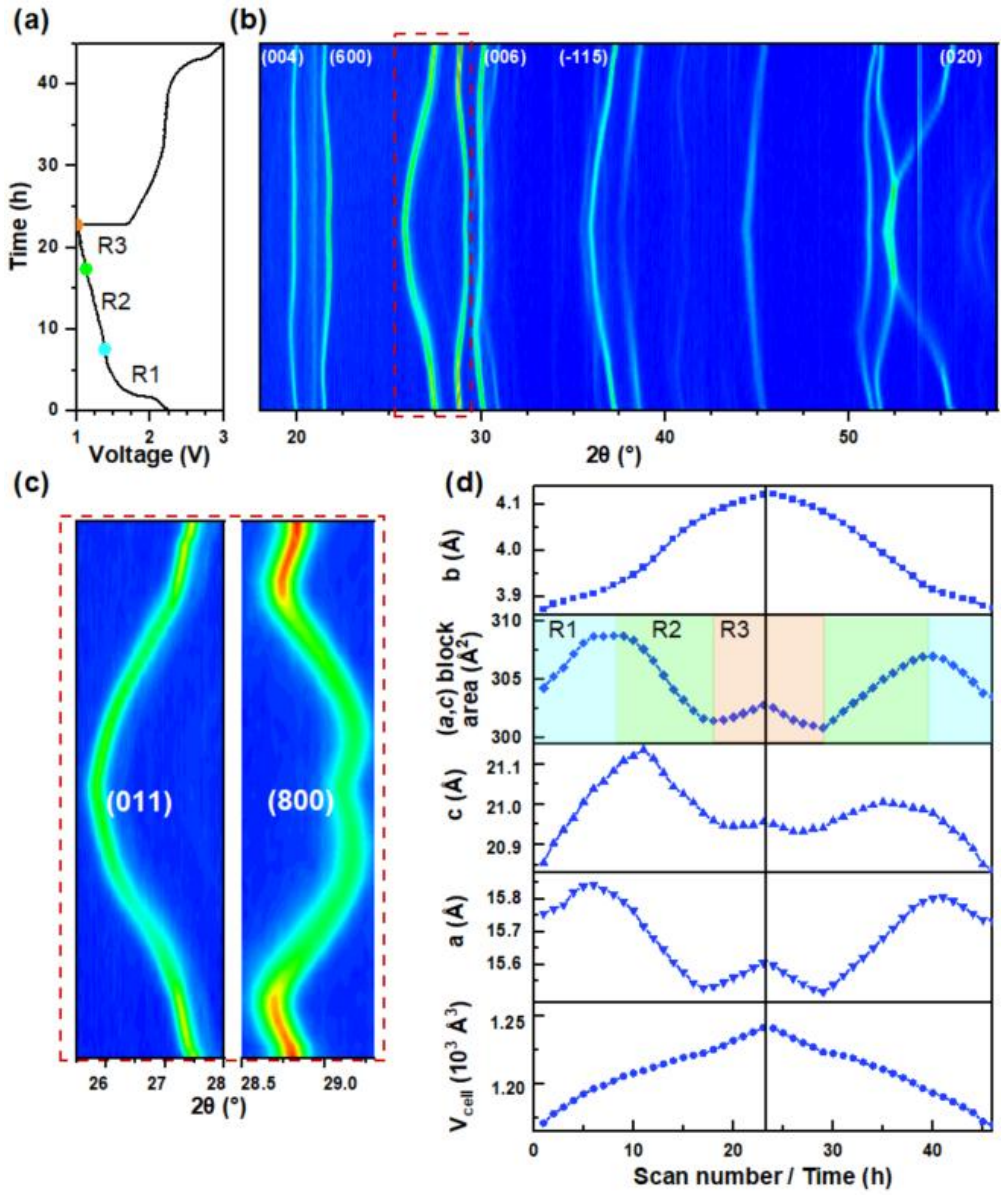

Figure 5. *The charge-discharge curve (a) and corresponding 2-dimensional contour plot of operando XRPD patterns for monoclinic* $FeNb_{11}O_{29}$ *(b), magnified view of (800) and (011) reflections (c), and the evolution of lattice parameters, (a,c) block area and unit cell volume during cycling (d).*

4. Conclusions

The Wadsley-Roth polymorphs of $FeNb_{11}O_{29}$ were successful and rapidly synthesized by microwave-assisted solid-state synthesis. This method presents significant benefits, including remarkably shorter time and limited particle growth, which turns to facilitate lithium-ion diffusion as evidenced by GITT coupled with differential capacity curves and *operando* XRPD. This easier ionic diffusion in turn induces enhanced rate capability and long-term cycling, with a high capacity of 179 mAh g^{-1} (90 % retention) after 500 cycles at 2 A g^{-1} delivered by microwave-heated monoclinic sample obtained from submicrometric precursors. The effect of smaller particle size is also seen when comparing between the two polymorphs, where the monoclinic samples exhibit higher capacity than the larger-sized orthorhombic ones. These results open the possibility for more efficient and upscalable protocols for other Wadsley-Roth phases as well as other battery materials.

Acknowledgements

As a part of the DESTINY PhD program, this publication is acknowledged by funding from the European Union's Horizon2020 research and innovation programme under the Marie Skłodowska-Curie Actions COFUND (Grant Agreement #945357). A. Guiet is indebted to the platforms “Diffusion et Diffraction des rayons X” and “Electronic Microscopy” of IMMM, Le Mans Université. R. Berthelot thanks the French National Research Agency (STORE-EX Labex Project ANR-10-LABX-76-01).

References

[1] Z. Chen, Y. Qin, Y. Ren, W. Lu, C. Orendorff, E.P. Roth, K. Amine, Multi-scale study of thermal stability of lithiated graphite, Energy Environ. Sci. 4 (2011) 4023–4030. https://doi.org/10.1039/C1EE01786A.

[2] B. Zhao, R. Ran, M. Liu, Z. Shao, A comprehensive review of $Li_4Ti_5O_{12}$-based electrodes for lithium-ion batteries: The latest advancements and future perspectives, Mater. Sci. Eng. R Rep. 98 (2015) 1–71. https://doi.org/10.1016/j.mser.2015.10.001.

[3] S. Andersson, J. Galy, Wadsley defects and crystallographic shear in hexagonally close-packed structures, J. Solid State Chem. 1 (1970) 576–582. https://doi.org/10.1016/0022-4596(70)90144-1.

[4] J.G. Allpress, R.S. Roth, The effect of annealing on the concentration of Wadsley defects in the Nb_2O_5-WO_3 system, J. Solid State Chem. 3 (1971) 209–216. https://doi.org/10.1016/0022-4596(71)90030-2.

[5] S. Iijima, J.G. Allpress, High resolution electron microscopy of $TiO_2 \cdot 7Nb_2O_5$, J. Solid State Chem. 7 (1973) 94–105. https://doi.org/10.1016/0022-4596(73)90127-8.

[6] S. Kimura, Phase equilibria in the system NbO_2-Nb_2O_5: Phase relations at 1300 and 1400°C and related thermodynamic treatment, J. Solid State Chem. 6 (1973) 438–449. https://doi.org/10.1016/0022-4596(73)90236-3.

[7] Y. Yang, J. Zhao, Wadsley–Roth Crystallographic Shear Structure Niobium-Based Oxides: Promising Anode Materials for High-Safety Lithium-Ion Batteries, Adv. Sci. 8 (2021) 2004855. https://doi.org/10.1002/advs.202004855.
[8] S. Patoux, M. Dolle, G. Rousse, C. Masquelier, A Reversible Lithium Intercalation Process in an ReO_3-Type Structure PNb_9O_{25}, J. Electrochem. Soc. 149 (2002) A391–A400. https://doi.org/10.1149/1.1455647.
[9] M.B. Preefer, M. Saber, Q. Wei, N.H. Bashian, J.D. Bocarsly, W. Zhang, G. Lee, J. Milam-Guerrero, E.S. Howard, R.C. Vincent, B.C. Melot, A. Van der Ven, R. Seshadri, B.S. Dunn, Multielectron Redox and Insulator-to-Metal Transition upon Lithium Insertion in the Fast-Charging, Wadsley-Roth Phase PNb_9O_{25}, Chem. Mater. 32 (2020) 4553–4563. https://doi.org/10.1021/acs.chemmater.0c00560.
[10] J.-T. Han, Y.-H. Huang, J.B. Goodenough, New Anode Framework for Rechargeable Lithium Batteries, Chem. Mater. 23 (2011) 2027–2029. https://doi.org/10.1021/cm200441h.
[11] C.P. Koçer, K.J. Griffith, C.P. Grey, A.J. Morris, Cation Disorder and Lithium Insertion Mechanism of Wadsley–Roth Crystallographic Shear Phases from First Principles, J. Am. Chem. Soc. 141 (2019) 15121–15134. https://doi.org/10.1021/jacs.9b06316.
[12] K. McColl, K.J. Griffith, R.L. Dally, R. Li, J.E. Douglas, K.R. Poeppelmeier, F. Corà, I. Levin, M.M. Butala, Energy storage mechanisms in vacancy-ordered Wadsley–Roth layered niobates, J. Mater. Chem. A. 9 (2021) 20006–20023. https://doi.org/10.1039/D1TA02992D.
[13] M.W. Logan, D. Zhang, B. Tan, K. Gerasopoulos, A scalable aluminum niobate anode for high energy, high power practical lithium-ion batteries, J. Mater. Chem. A. 9 (2021) 11228–11240. https://doi.org/10.1039/D1TA00613D.
[14] X. Lou, R. Li, X. Zhu, L. Luo, Y. Chen, C. Lin, H. Li, X.S. Zhao, New Anode Material for Lithium-Ion Batteries: Aluminum Niobate ($AlNb_{11}O_{29}$), ACS Appl. Mater. Interfaces. 11 (2019) 6089–6096. https://doi.org/10.1021/acsami.8b20246.
[15] X. Lou, Q. Fu, J. Xu, X. Liu, C. Lin, J. Han, Y. Luo, Y. Chen, X. Fan, J. Li, $GaNb_{11}O_{29}$ Nanowebs as High-Performance Anode Materials for Lithium-Ion Batteries, ACS Appl. Nano Mater. 1 (2018) 183–190. https://doi.org/10.1021/acsanm.7b00091.
[16] Z. Wang, R. Zheng, Y. Li, H. Yu, J. Zhang, X. Zhang, W. Bi, M. Shui, J. Shu, Synthesis and characterization of $GaNb_{11}O_{29}$@C for high-performance lithium-ion battery, Ceram. Int. 46 (2020) 5913–5919. https://doi.org/10.1016/j.ceramint.2019.11.044.
[17] I. Pinus, M. Catti, R. Ruffo, M.M. Salamone, C.M. Mari, Neutron Diffraction and Electrochemical Study of $FeNb_{11}O_{29}$/ $Li_{11}FeNb_{11}O_{29}$ for Lithium Battery Anode Applications, Chem. Mater. 26 (2014) 2203–2209. https://doi.org/10.1021/cm500442j.
[18] P. Tabero, Synthesis and properties of $FeNb_{11}O_{29}$, Ceram. - Silik. 49 (2005) 126–131.
[19] D. Spada, M.C. Mozzati, B. Albini, P. Galinetto, I. Quinzeni, D. Capsoni, M. Bini, Deepening the shear structure $FeNb_{11}O_{29}$: influence of polymorphism and doping on structural, spectroscopic and magnetic properties, Dalton Trans. 47 (2018) 15816–15826. https://doi.org/10.1039/C8DT02896F.
[20] D. Spada, I. Quinzeni, M. Bini, Orthorhombic and monoclinic modifications of $FeNb_{11}O_{29}$, as promising anode materials for lithium batteries: Relationships between pseudocapacitive behaviour and structure, Electrochimica Acta. 296 (2019) 938–944. https://doi.org/10.1016/j.electacta.2018.11.047.
[21] D. Spada, B. Albini, P. Galinetto, D. Versaci, C. Francia, S. Bodoardo, G. Bais, M. Bini, $FeNb_{11}O_{29}$, anode material for high-power lithium-ion batteries: Pseudocapacitance and symmetrisation unravelled with advanced electrochemical and in situ/operando techniques, Electrochimica Acta. 393 (2021) 139077. https://doi.org/10.1016/j.electacta.2021.139077.
[22] D. Spada, M. Aramini, M. Fittipaldi, A. Cini, M. Fracchia, P. Ghigna, A. Girella, C. Milanese, M. Bini, Spectroscopic Techniques and DFT Calculations to Highlight the Effect of Fe^{3+} on the Properties of

$FeNb_{11}O_{29}$, Anode Material for Lithium-Ion Batteries, J. Phys. Chem. C. 126 (2022) 4698–4709. https://doi.org/10.1021/acs.jpcc.1c10573.
[23] Y. Yang, H. Zhu, F. Yang, F. Yang, D. Chen, Z. Wen, D. Wu, M. Ye, Y. Zhang, J. Zhao, Q. Liu, X. Lu, M. Gu, C.C. Li, W. He, Ten Thousand-Cycle Ultrafast Energy Storage of Wadsley–Roth Phase Fe–Nb Oxides with a Desolvation Promoting Interfacial Layer, Nano Lett. 21 (2021) 9675–9683. https://doi.org/10.1021/acs.nanolett.1c03478.
[24] Z. Lv, H. Zhu, W. Meng, L. Wei, Y. Yang, Y. Zhang, M. Ye, C.C. Li, Cation mixing in Wadsley-Roth phase anode of lithium-ion battery improves cycling stability and fast Li^+ storage, Appl. Phys. Rev. 8 (2021) 031404. https://doi.org/10.1063/5.0054030.
[25] M. Bini, I. Quinzeni, D. Spada, The Doping of $FeNb_{11}O_{29}$ as a Way to Improve Its Electrochemical Performances, ChemistrySelect. 4 (2019) 5656–5661. https://doi.org/10.1002/slct.201901182.
[26] X. Lou, C. Lin, Q. Luo, J. Zhao, B. Wang, J. Li, Q. Shao, X. Guo, N. Wang, Z. Guo, Crystal Structure Modification Enhanced $FeNb_{11}O_{29}$ Anodes for Lithium-Ion Batteries, ChemElectroChem. 4 (2017) 3171–3180. https://doi.org/10.1002/celc.201700816.
[27] R. Zheng, S. Qian, X. Cheng, H. Yu, N. Peng, T. Liu, J. Zhang, M. Xia, H. Zhu, J. Shu, $FeNb_{11}O_{29}$ nanotubes: Superior electrochemical energy storage performance and operating mechanism, Nano Energy. 58 (2019) 399–409. https://doi.org/10.1016/j.nanoen.2019.01.065.
[28] E.E. Levin, J.H. Grebenkemper, T.M. Pollock, R. Seshadri, Protocols for High Temperature Assisted-Microwave Preparation of Inorganic Compounds, Chem. Mater. 31 (2019) 7151–7159. https://doi.org/10.1021/acs.chemmater.9b02594.
[29] F. Murgia, P. Antitomaso, L. Stievano, L. Monconduit, R. Berthelot, Express and low-cost microwave synthesis of the ternary Chevrel phase $Cu_2Mo_6S_8$ for application in rechargeable magnesium batteries, J. Solid State Chem. 242 (2016) 151–154. https://doi.org/10.1016/j.jssc.2016.07.022.
[30] K.K. Gupta, K. Li, S. Balaji, P.S. Kumar, C. Lu, Microwave-assisted synthesis and electrochemical characterization of $TiNb_2O_7$ microspheres as anode materials for lithium-ion batteries, J. Am. Ceram. Soc. (2023) jace.19000. https://doi.org/10.1111/jace.19000.
[31] V.C. Wu, H.A. Evans, R. Giovine, M.B. Preefer, J. Ong, E. Yoshida, P. Cabelguen, R.J. Clément, Rapid and Energy-Efficient Synthesis of Disordered Rocksalt Cathodes, Adv. Energy Mater. 13 (2023) 2203860. https://doi.org/10.1002/aenm.202203860.
[32] P. Aswathy, S. Suriyakumar, S.A. Kumar, M.S. Oliyantakath Hassan, V. Vijayan, M.M. Shaijumon, Microwave-Assisted Synthesis of Sulfide Solid Electrolytes for All-Solid-State Sodium Batteries, ACS Appl. Energy Mater. 5 (2022) 12592–12601. https://doi.org/10.1021/acsaem.2c02224.